applied sciences

MDPI

Article

Prediction of Douglas-Fir Lumber Properties: Comparison between a Benchtop Near-Infrared Spectrometer and Hyperspectral Imaging System

Laurence Schimleck [1,*], Joseph Dahlen [2], Seung-Chul Yoon [3], Kurt C. Lawrence [3] and Paul David Jones [4]

1 Wood Science and Engineering, Oregon State University, Corvallis, OR 97331, USA
2 Warnell School of Forestry and Natural Resources, University of Georgia, Athens, GA 30602, USA; jdahlen@uga.edu
3 Agricultural Research Service, United States Department of Agriculture, Athens, GA 30605, USA; SeungChul.Yoon@ars.usda.gov (S.-C.Y.); kurt.lawrence@ars.usda.gov (K.C.L.)
4 Benchmark International, Eugene, OR 97402, USA; clemsonforest@gmail.com
* Correspondence: Laurence.Schimleck@oregonstate.edu

Received: 16 November 2018; Accepted: 10 December 2018; Published: 12 December 2018

Featured Application: Hyperspectral imaging may provide lumber mills with a cost-effective method to efficiently identify areas of high and low stiffness within logs prior to sawing, and thus allow mills to make more informed decisions on a log-by-log basis for sawing solutions.

Abstract: Near-infrared (NIR) spectroscopy and NIR hyperspectral imaging (NIR-HSI) were compared for the rapid estimation of physical and mechanical properties of No. 2 visual grade 2 × 4 (38.1 mm by 88.9 mm) Douglas-fir structural lumber. In total, 390 lumber samples were acquired from four mills in North America and destructively tested through bending. From each piece of lumber, a 25-mm length block was cut to collect diffuse reflectance NIR spectra and hyperspectral images. Calibrations for the specific gravity (SG) of both the lumber (SG_{lumber}) and 25-mm block (SG_{block}) and the lumber modulus of elasticity (MOE) and modulus of rupture (MOR) were created using partial least squares (PLS) regression and their performance checked with a prediction set. The strongest calibrations were based on NIR spectra; however, the NIR-HSI data provided stronger predictions for all properties. In terms of fit statistics, SG_{block} gave the best results, followed by SG_{lumber}, MOE, and MOR. The NIR-HSI SG_{lumber}, MOE, and MOR calibrations were used to predict these properties for each pixel across the transverse surface of the scanned samples, allowing SG, MOE, and MOR variation within and among rings to be observed.

Keywords: bending stiffness; bending strength; NIR; nondestructive testing; *Pseudotsuga menziesii*; wood and fiber quality

1. Introduction

The Northwestern United States accounts for a large proportion of the structural lumber produced in the United States, to which Douglas-fir (*Pseudotsuga menziesii* (Mirb.) Franco) is the most important species [1,2]. Douglas-fir is increasingly being sourced from forest plantations that yield excellent growth, which allows for shorter rotation lengths than in the past [3–6]. The wood from stands harvested from short rotations have a higher proportion of corewood (juvenile wood), which has a lower modulus of elasticity (MOE or stiffness), lower modulus of rupture (MOR or strength), and lower dimensional stability compared to wood harvested from older stands [7–9].

Due to the variable nature of wood, there is a need to better segregate high-quality material from low-quality material. Prior to sawing logs into lumber, logs can be evaluated by measuring the acoustic velocity, with high velocity indicating stiffer wood than logs with low velocity [10–14]. Segregating logs by acoustic velocity has its limitations in that logs with low acoustic velocity can contain lumber with high stiffness and vice versa, because much of the variation in stiffness within a log is due to the radial variability associated with corewood and outerwood variation [15,16]. Once sawn into lumber, the stiffness of a piece can be assessed by measuring the density and the acoustic velocity [8,17]; however, at this point, the lumber has already been sawn and thus the product has been determined. Changing the product after sawing would generate significant waste and thus is not common. Thus, improved methods for measuring wood properties are needed at the log level for more informed decision-making within a lumber mill. At a veneer mill, the same challenges exist and the use of segregating logs by acoustic velocity has been applied successfully to poplar (*Populus euramericana*) [18] and trembling aspen (*Populus tremuloides* Michx.) [19].

Near-infrared (NIR) spectroscopy has emerged as an alternative approach for the estimation of mechanical properties of lumber. In studies based on short, defect-free samples, the potential of NIR spectroscopy for predicting density, MOE, and MOR in both softwoods [20–23] and hardwoods [24] has been demonstrated. These studies on small clear samples represent a "best-case" scenario, as a small number of spectra can adequately represent a sample due to the limited radial and vertical variation found in a small clear sample. Owing to size and variability, the collection of representative spectra from dimensional lumber of standard size presents a far greater challenge. Dahlen et al. [25] reviewed publications that had explored estimation of the mechanical properties of softwood lumber [26–30]. Of these studies, only Hoffmeyer and Pedersen [26] collected spectra from the transverse surface; all others scanned along the length of the sample with spectra collected from the tangential and/or radial face. Calibration and prediction statistics were variable, with the strongest predictions (R_p^2 = 0.82) reported for hinoki cypress (*Chamaecyparis obtusa* (Siebold & Zucc.) lumber [30]. Only Fujimoto et al. [29] reported a calibration for MOR, and it was much weaker than that reported for MOE using the same set of Japanese larch (*Larix kaempferi* (Lamb.) Carr.) lumber.

Dahlen et al. [25] utilized transverse face spectra collected from a laboratory-grade NIR spectroscopy instrument to predict the SG, MOE, and MOR of No. 2 grade 2 × 4 southern pine lumber from six commercial mills in the Southeast. The Duplex sample selection technique was used to identify samples for the calibration (539) and prediction (179) sets. Moderate results were reported for the prediction set for lumber SG (R_p^2 = 0.53), MOE (R_p^2 = 0.58), and MOR (R_p^2 = 0.4). There, the spectra were collected from approximately 8% of the area of the transverse face, but the prediction statistics were quite favorable compared to full-length density information collected from the lumber (MOE R^2 = 0.46, MOR R^2 = 0.51). These NIR results were promising, especially given the limited area in which the NIR spectra was collected, and the authors proposed that the use of an NIR instrument that allowed a larger area of the transverse surface to be scanned could provide better results.

To this end, NIR hyperspectral imaging (HSI) is an emerging methodology whose use has been reported in several recent reviews across a range of fields, including medical applications [31], food quality and safety [32,33], and plants and biological materials [34,35]. As noted by Burger and Gowen [36], "HSI combines spectroscopy and imaging, resulting in three-dimensional multivariate data structures ('hypercubes'). Each pixel in a hypercube contains a spectrum representing its light absorbing and scattering properties. This spectrum can be used to estimate the chemical composition and/or physical properties of the spatial region represented by that pixel.". NIR-HSI can thus be used to capture information on the spatial distribution of wood properties [34], and to this end, it provides an option for the collection of spectra over the entire transverse surface of the lumber. In addition, all spectra collected from the surface of an individual sample can be averaged to a single spectrum that represents the whole area scanned.

The earliest related HSI studies on wood used visible light [37,38] and wavelengths from 400–1000 nm [39] to detect compression wood. Jones et al. [40] utilized NIR-HSI data from

1250–1650 nm to estimate density, microfibril angle (MFA), and stiffness pith-to-bark variation at 2-mm spatial resolution for loblolly pine (*Pinus taeda* L.). More recently, Fernandes et al. [41,42] estimated density for stone pine (*Pinus pinea* L.), while Ma et al. [43] reported maps of radial strips showing density and MFA variation at high spatial resolution for Sugi (*Cryptomeria japonica* (L.f.) D. Don). Thumm et al. [44,45] utilized NIR-HSI to examine the spatial variation of several radiata pine (*Pinus radiata* D. Don) wood properties (lignin, cellulose, hemicellulose, galactose, glucose) across discs, while for the same species, NIR-HSI has also been used to detect compression wood [46] and resin defects [47]. Mora et al. [48] utilized NIR-HSI to estimate loblolly pine whole-log density and moisture content. Due to the flexibility of NIR-HSI, the system has many possible applications in manufacturing environments. Whole-board maps showing variation in moisture content [49] and density [50] were reported for subalpine fir (*Abies lasiocarpa* Hook) lumber. Lestander et al. [51] used NIR-HSI to identify wood chips with high levels of extractives, which would allow for biomass to be directed towards a process stream that would maximize its utilization.

The advantages of NIR-HSI are apparent, but compared to benchtop NIR systems, there is typically a higher interval between wavelengths and the signal-to-noise ratio may not be as high, thus the calibrations may not be as accurate as those of a benchtop system. Hence, the primary goals of this preliminary study were to (1) compare the use of NIR spectroscopy with NIR-HSI on Douglas-fir lumber properties with the transverse face scanned on both instruments, (2) compare the predictions with models constructed to predict MOE and MOR using specific gravity, and (3) utilize the NIR-HSI for the spatial prediction of properties on transverse surfaces. If successful and with additional studies, the flexibility of the NIR-HSI could potentially be used in a mill, whereby logs could be scanned and areas within a log that do not meet product specifications could have their sawing pattern changed to a more suitable product.

2. Materials and Methods

2.1. Specimen Preparation and Testing

Four packages of kiln-dried No. 2 grade, 2 × 4 (38 mm × 89 mm × 2438 mm) Douglas-fir (DF) lumber were obtained from commercial mills in Canada, Idaho, Oregon, and Washington [52]. From each of the four mills, 124 pieces were originally tested, for a total of 496 samples. For each lumber specimen, the dimensions, weight, and moisture content were measured. The specific gravity at 15% moisture content (SG_{lumber}) was determined for the lumber. Following testing, a block (38 mm by 89 mm by 51 mm longitudinally) was cut from the lumber using a radial arm saw. Not all pieces yielded a usable sample for the NIR and HSI analysis due to a number of reasons, including the failure of the piece due to shear which split the piece in half, along with other testing-related failures, and some samples were excluded due to excessive cracking. Thus, a total of 390 pieces were available for the NIR and HSI analysis, with 88 samples from Canada, 95 samples from Idaho, 109 samples from Oregon, and 98 samples from Washington. The lumber represents a wide range of variability that is found in commerce (Figure 1). The specific gravity at 12% moisture content (SG_{block}) was then determined for the block. The edgewise destructive bending test setup was conducted via four-point bending in third-point loading (load heads positioned one-third of the span distance from the reactions) on an Instron Satec testing machine [53,54]. The span-to-depth ratio was 21:1 (1867 mm to 89 mm). The tension face of each sample was randomly selected, and if a strength-reducing defect was identified, it was located randomly between the reaction points [53]. Deflection was measured using a Tinius Olsen deflectometer to determine MOE; MOR was calculated from the maximum load. MOE and MOR were adjusted to 15% moisture content [52,55].

2.2. Near-Infrared Spectroscopy

Diffuse reflectance NIR spectra were collected from the cross-sectional face of each block using a FOSS NIR Systems Inc. Model 5000 scanning spectrometer (FOSS NIRSystems Inc. Laurel, MD, USA).

A 16.5 mm by 16.5 mm white Teflon mask was installed on the face of the spectrometer to ensure that a consistent section was scanned. All measurements were made in a controlled environment of 40% relative humidity and a temperature of 20 °C. The spectra were collected at 2-nm intervals over the wavelength range 1100–2500 nm. The instrument reference was a ceramic standard. Two separate scans were conducted on each piece with each scan being an average of 32 readings; the two scans were then averaged to give a single spectrum per block.

Figure 1. Transverse view of randomly selected lumber pieces from the study.

2.3. Hyperspectral Imaging

Hyperspectral images were collected on a push broom short-wave infrared (SWIR) system (Hyperspec ® SWIR, Headwall Photonics, Fitchburg, MA, USA) in the wavelength range 1000–2500 nm. The system (Figure 2) consisted of a spectrograph, a focal plane array with a Peltier-cooled 320 × 256 mercury cadmium telluride (MCT) detector (MCT-851 XC403, Xenics, Leuven, Belgium), a 30.7-mm front lens (OLES30, Specim, Oulu, Finland), two illumination sources with tungsten halogen lamps, a motorized linear slide (T-LSR300B, Zaber Technologies, Vancouver, BC, Canada), a computer, and in-house developed software (C++) for image acquisition and preprocessing, including intensity calibration and denoising. Two light sources oriented approximately 20 degrees from the sample were used for illumination. For each image, a scan of an individual sample started while a dark current reference was collected with the camera lens cap covering the lens. After acquiring about 10 lines of dark current signals, the lens cap was opened so that white reference signals were collected from a white diffuse-reflectance standard panel (Fluorilon-99W, Avian Technologies, Sunapee, NH, USA) with dimensions 25 mm × 300 mm, followed by scanning of sample (Figure 2). The spectra were collected at approximately 8-nm intervals over the wavelength range 1000–2500 nm. Due to the intensity of light, care was taken to not leave samples exposed to the light beyond the sample collection period. The background plate was stationary and black.

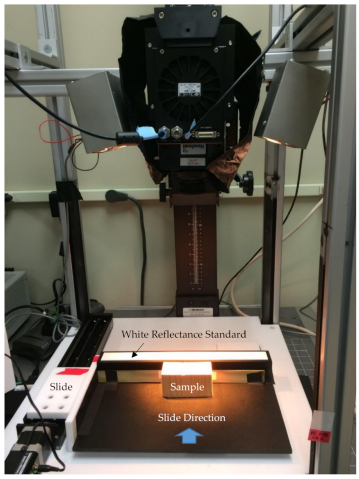

Figure 2. Hyperspectral imaging setup.

2.4. Hyperspectral Imaging Data Processing

The raw hyperspectral data was calibrated to relative reflectance (R) via an in-field calibration process, where the dark current and white references were averaged to two horizontal reference lines. Each image was calibrated with its own dark current and white reference signals. Then, the relative reflectance values were transformed to absorbance (A), with the equation $A = \log_{10} 1/R$. Then, these absorbance spectral images were used for subsequent data analysis. The hyperspectral data processing was done with custom Matlab scripts. The wavelength range of the calibrated data was cropped to 1100–2500 nm. The white reference image in the top of each image was removed and the bottom edge of each sample was also removed, which was automatically done with an image-processing algorithm based on edge detection and image segmentation. Intensity thresholding was used for the image segmentation of an individual sample. Then, a region of interest (ROI) with a rectangular shape was automatically detected inside each segmentation image of an individual sample. The ROIs were automatically detected by an image-processing algorithm in Matlab. More specifically, note that a measured hyperspectral image consisted of three sections, i.e., dark current, white target, and sample sections, from top to bottom. A waveband at 1789 nm in the approximately middle of the measured spectral range was chosen to find three horizontal line edges dividing three sections via a y-profile analysis technique. A y-profile was obtained by projecting the 2-D waveband image onto the y-axis and averaging all intensity values along each y point. Then, the first derivative was applied to the y profile and the peaks were searched to find y edges of the dark current, white target, and sample. After the sample's y edges (top and bottom edges) were detected, its left and right edges were detected similarly by a x-profile analysis technique such that the sample became segmented and enclosed by a bounding box obtained from the coordinates of the detected four edges. An ROI was detected inside this bounding box by shrinking the bounding box of the sample by 8% and 5% in the y and x directions, respectively. These ROIs were used to extract spectral data for analysis.

2.5. Wood Property Calibration and Prediction of Wood Properties

Wood property calibrations, statistical analyses, and associated graphics were developed using the R statistical software [56] with the RStudio interface [57] and the packages gridExtra [58], pls [59], prospectr [60], signal [61], and the tidyverse series of packages [62]. Models were developed between MOE and MOR with SG_{lumber}, and MOR with MOE. Linear models were developed between MOR and MOE [52]. Examining the scatterplots between MOE and MOR with SG_{lumber} showed that the relationships were not linear; several model forms were tested, with the best models being quadratic models without the linear term. For these models, the coefficient of determination (R^2) and the root mean square error (RMSE) were calculated.

For both the NIR and the NIR-HSI spectra, the pretreatment used was the second derivative with the left and right gaps of four points using the Savitzky–Golay approach [63]. The samples were split into the calibration set, which contained 75% of the samples (292 samples), and the prediction set which contained the remaining 25% (98 samples) of the sets using the Duplex sample selection technique done on the NIR spectra data [60]. The duplex algorithm selects the most unique samples based on the Mahalanobis distance to better ensure that the calibration and prediction set contain samples that are representative of the population, while still maintaining independence between the calibration and prediction sets [64,65].

The specific gravity of the block (SG_{block}), specific gravity of the entire lumber piece adjusted to 15% moisture content (SG_{lumber}), modulus of elasticity adjusted to 15% moisture content (MOE), and modulus of rupture adjusted to 15% moisture content (MOR) were modeled as responses to the NIR and the NIR-HSI spectra. Calibrations were developed using partial least square (PLS) regression with four cross-validation segments and a maximum of 10 factors. The final number of factors were determined based on the standard error of cross-validation (SECV) (determined from the residuals of the final cross-validation), the root mean square error of cross-validation (RMSECV), the coefficient of determination of cross-validation (R^2), and the ratio of performance to deviation for the cross-validation

(RPDcv) [66]. RPDcv was calculated as the ratio of the standard deviation of the reference data to the SECV. Determination of the RPDcv allows the comparison of calibrations developed for different wood properties that have differing data ranges and units; the higher the RPDcv, the more accurately the data is described by the calibration. The performance of the calibration models was examined by predicting the wood properties of the test set samples. The standard error of prediction (SEP) (determined from the residuals of the predictions) was calculated and gives a measure of how well a calibration predicts parameters of interest for a set of samples not included in the calibration set. The predictive ability of the calibrations was assessed by the coefficient of determination (R_p^2) and calculating the RPDp, which is similar to the RPDcv, but uses the standard deviation of the prediction set reference data and the SEP. The bias (mean of prediction residuals) was also evaluated. Plots were produced to show the relationship between the measured data with the NIR or NIR-HSI data, with the plots also showing the confidence interval for the mean prediction and the 1:1 line of equivalence.

Following the creation of the PLS NIR-HSI models, the coefficients of the PLS model were used to predict the spatial variation within each block for SG, MOE, and MOR in Matlab. This work was similar to a calibration transfer from a spectrometer to a hyperspectral imaging system, done in Matlab. The pretreatment (Savitzky–Golay filtering) process was exactly replicated in Matlab. Spectral data in each image were folded to a matrix form. The PLS model coefficients in a CSV-format file (in Supplementary Materials) were read and applied to the spectrum in each pixel via a matrix form. The output results were refolded back to an image domain, where each pixel contained prediction values for SG, MOE or MOR, depending on a PLSR model. Finally, the prediction images were converted to pseudo-color, where each pixel value was represented with a standardized color.

3. Results

Table 1 contains the property measurements for the lumber utilized in the current study, broken down by calibration data set and prediction data set. The SG, MOE, and MOR data is highly variable, which reflects the variability that these properties have in commerce. Both data sets contained samples with similar summary statistics for each property, which meant that the Duplex sample selection algorithm successfully selected calibration and prediction samples across the range of values only using information from the NIR spectra.

Table 1. Summary statistics of block specific gravity, lumber specific gravity, lumber modulus of elasticity, and lumber modulus of rupture for calibration and prediction sets.

	Calibration					Prediction				
Property [1]	**N**	**Mean**	**Min**	**Max**	**SD**	**N**	**Mean**	**Min**	**Max**	**SD**
SG_{block}	292	0.455	0.326	0.667	0.066	98	0.459	0.343	0.626	0.067
SG_{lumber}		0.47	0.346	0.619	0.051		0.472	0.374	0.603	0.05
MOE		12	6.3	19.9	2.8		12	6.5	20.4	2.9
MOR		44.6	14.8	93.6	16.2		44.5	13.4	94.3	17.8

[1] SG_{block} = block specific gravity, SG_{lumber} = lumber specific gravity, MOE = modulus of elasticity (GPa), MOR = modulus of rupture (MPa).

A reference point for comparing the relative performance of the NIR and NIR-HSI systems to model MOE and MOR is to compare them against predictions using the measured SG of the lumber, and for MOR, the measured static MOE (Figure 3). A quadratic regression model without the linear term was used to model MOE versus lumber SG (intercept = 3.7, parameter = 37.1), which had a coefficient of determination of 0.42 and a root mean square error (RMSE) of 2.1 GPa. The same model form was used to model MOR versus lumber SG (intercept = −3.6, parameter = 215.4), which had a coefficient of determination of 0.41 and a RMSE of 12.8 MPa. For both models, the quadratic model form instead of a linear model was used because of the differences in the radial variation trends for wood properties of Douglas-fir. Wood density decreases for approximately 8 years from pith to bark and then increases, whereas stiffness and strength increases from pith to bark because of decreasing microfibril angle [67]. Thus, for samples near the pith, a lower density value does not necessarily

mean a decrease in wood stiffness or strength. A linear model was used to model MOR versus MOE (intercept = −14.8, parameter = 4.9), which had a coefficient of determination value of 0.69 and a root mean square error (RMSE) value of 9.2 MPa.

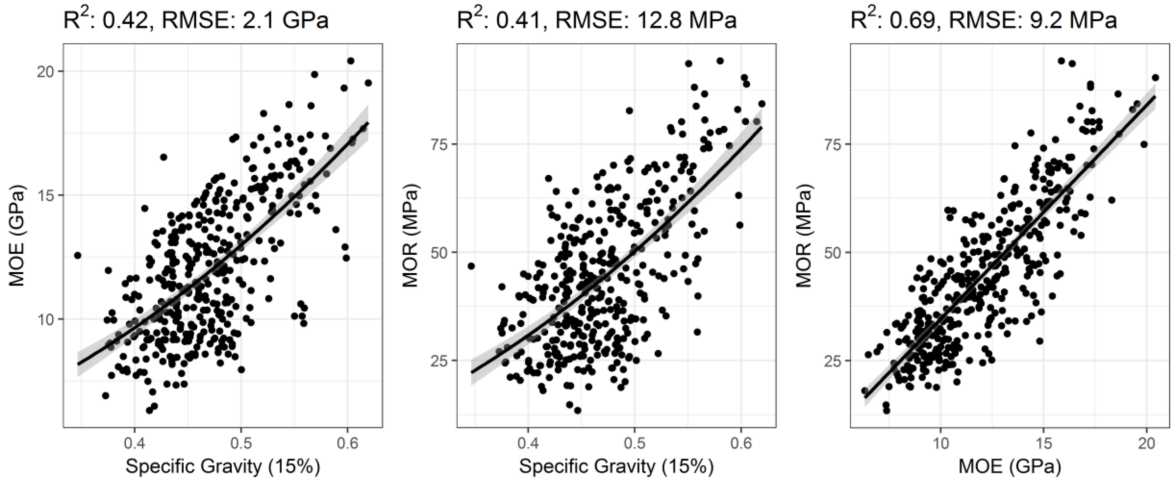

Figure 3. Quadratic and linear models and plots to predict modulus of elasticity (MOE) and modulus of rupture (MOR) with lumber specific gravity and MOE. RMSE: root mean square error.

Table 2 contains the results of the calibration models and their predictions for the various properties measured in the study using second-derivative NIR spectra. The PLS coefficients for the intercept and the wavelengths are included as supplementary data. All of the RPDp results are lower than what is frequently cited by AACC Method 39-00 [68] as the recommended values for screening in breeding programs (RPD > 2.5), but these guidelines were set up for cereal grains and not for translating wood chemistry information as detected by the NIR spectra to that of the physical and mechanical properties of wood. For the block SG (SG_{block}), 10 factors were chosen for the cross-validation for the NIR model, and 6 factors for the NIR-HSI model. When used to predict SG_{block}, the NIR model gave a R_p^2 of 0.78 and a SEP of 0.031, while the NIR-HSI gave a R_p^2 of 0.82 and a SEP of 0.029 (Figure 4). The bias was slightly higher for the NIR-HSI model than for the NIR model. For the lumber SG (SG_{lumber}), 10 factors were chosen for the cross-validation for the NIR model and 7 factors for the NIR-HSI model. When used to predict SG_{lumber}, the NIR model gave a R_p^2 of 0.65 and a SEP of 0.029, while the NIR-HSI gave a R_p^2 of 0.70 and a SEP of 0.027 (Figure 5). The bias was slightly lower for the NIR-HSI model than the NIR model.

Table 2. Near-infrared spectroscopy and hyperspectral imaging results of block specific gravity, lumber specific gravity, lumber modulus of elasticity, and lumber modulus of rupture for the calibration and prediction sets.

		Calibration					Prediction			
Tool [1]	**Property [2]**	**No. Factors**	**R^2**	**SECV**	**RMSECV**	**RPDcv**	**R_p^2**	**SEP**	**RPDp**	**Bias**
NIR	SG_{block}	10	0.83	0.027	0.035	2.4	0.78	0.031	2.1	0.00075
	SG_{lumber}	10	0.74	0.026	0.032	2.0	0.65	0.029	1.7	0.0033
	MOE	6	0.67	1.6	1.8	1.7	0.56	1.9	1.5	0.16
	MOR	7	0.57	10.7	12.2	1.5	0.40	13.7	1.3	0.75
NIR-HSI	SG_{block}	6	0.75	0.033	0.037	2.0	0.82	0.029	2.3	0.0029
	SG_{lumber}	7	0.67	0.03	0.033	1.7	0.70	0.027	1.8	0.0013
	MOE	5	0.65	1.6	1.7	1.7	0.62	1.8	1.6	0.15
	MOR	6	0.51	11.3	12.2	1.4	0.49	12.7	1.4	0.79

[1] NIR = near-infrared spectroscopy, NIR-HSI = near-infrared spectroscopy hyperspectral imaging. [2] SG_{block} = block specific gravity, SG_{lumber} = lumber specific gravity, MOE = modulus of elasticity (GPa), MOR = modulus of rupture (MPa). SECV: standard error of cross-validation; RPDcv: ratio of performance to deviation for the cross-validation; R_p^2: R^2 for predictions of each property; SEP: standard error of prediction; RPDp: ratio of performance to deviation for the prediction set.

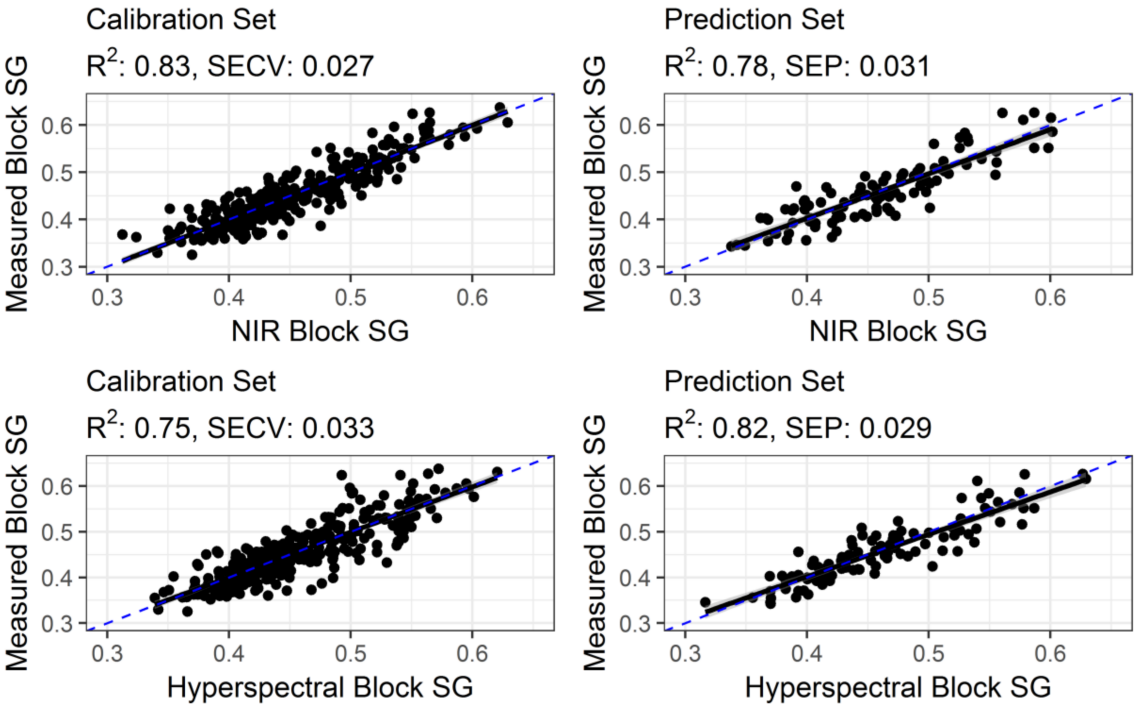

Figure 4. Calibration and prediction plots of block specific gravity for near-infrared spectroscopy and hyperspectral imaging. The dashed blue line indicates the line of equivalence.

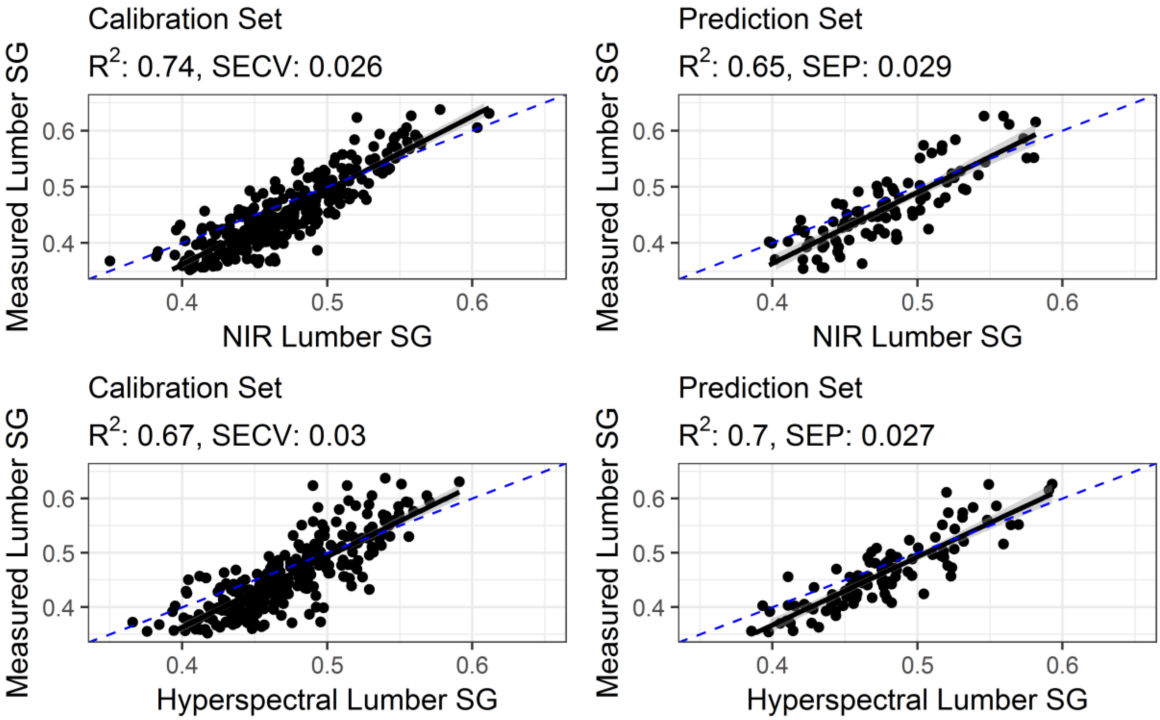

Figure 5. Calibration and prediction plots of lumber specific gravity for near-infrared spectroscopy and hyperspectral imaging. The dashed blue line indicates the line of equivalence.

For MOE, six factors were chosen for the cross-validated NIR model and five factors for the NIR-HSI model. When used to predict MOE, the NIR model gave a R_p^2 of 0.56 and a SEP of 1.9 GPa, while the NIR-HSI model was slightly better (R_p^2 = 0.62, SEP = 1.8 GPa) (Figure 6). The bias was similar for the NIR and the NIR-HSI models. For the NIR-based MOR calibration, seven factors were chosen,

while six factors were recommended for the NIR-HSI model. When used to predict MOR, the NIR model gave a R_p^2 of 0.40 and a SEP of 13.7 MPa, which was inferior to the NIR-HSI MOR model (R_p^2 = 0.49, SEP = 12.7 MPa) (Figure 7). The bias was similar for the NIR and the NIR-HSI models.

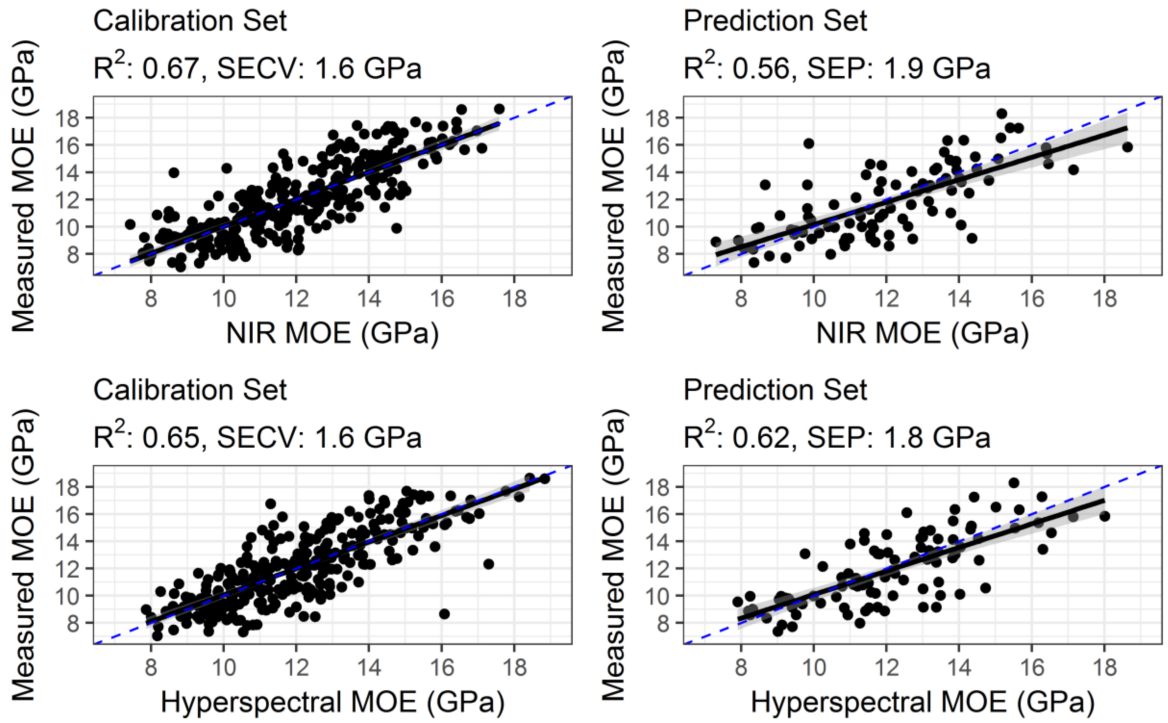

Figure 6. Calibration and prediction plots of modulus of elasticity (MOE) for near-infrared spectroscopy and hyperspectral imaging. The dashed blue line indicates the line of equivalence.

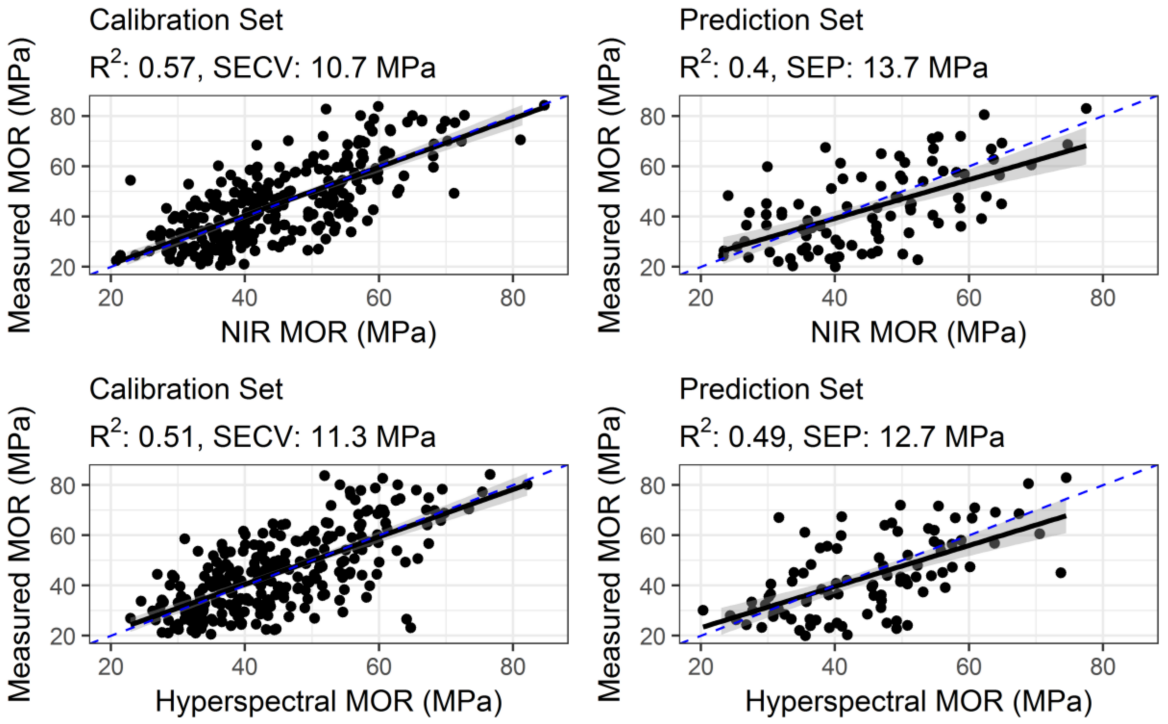

Figure 7. Calibration and prediction plots of modulus of rupture (MOR) for near-infrared spectroscopy and hyperspectral imaging. The dashed blue line indicates the line of equivalence.

The PLS model for the NIR-HSI system was then used to visualize the spatial variation in SG, MOE, and MOR. Figure 8 illustrates the predictions on a sample containing the pith with wide growth rings, thus being indicative of low-stiffness corewood, while Figure 9 illustrates the predictions on a sample containing narrow growth rings, thus being indicative of high-stiffness outerwood.

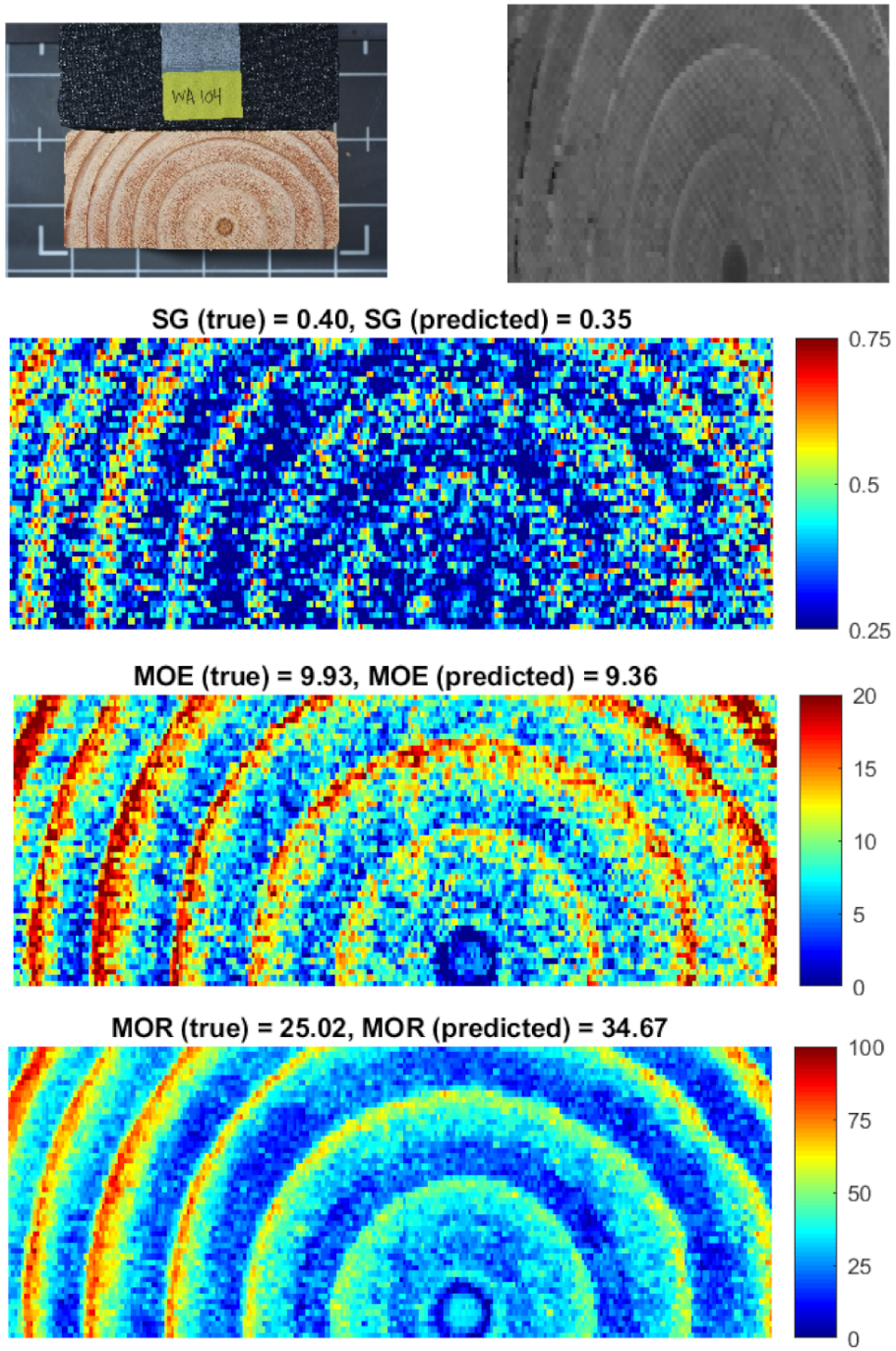

Figure 8. Top left: RGB image, **Top Right**: single hyperspectral channel image, **Bottom**: prediction of specific gravity (SG), modulus of elasticity (MOE) (GPa), and modulus of rupture (MOR) (MPa) using the partial least squares (PLS) models and applied to one sample in the study with wide growth rings and containing the pith.

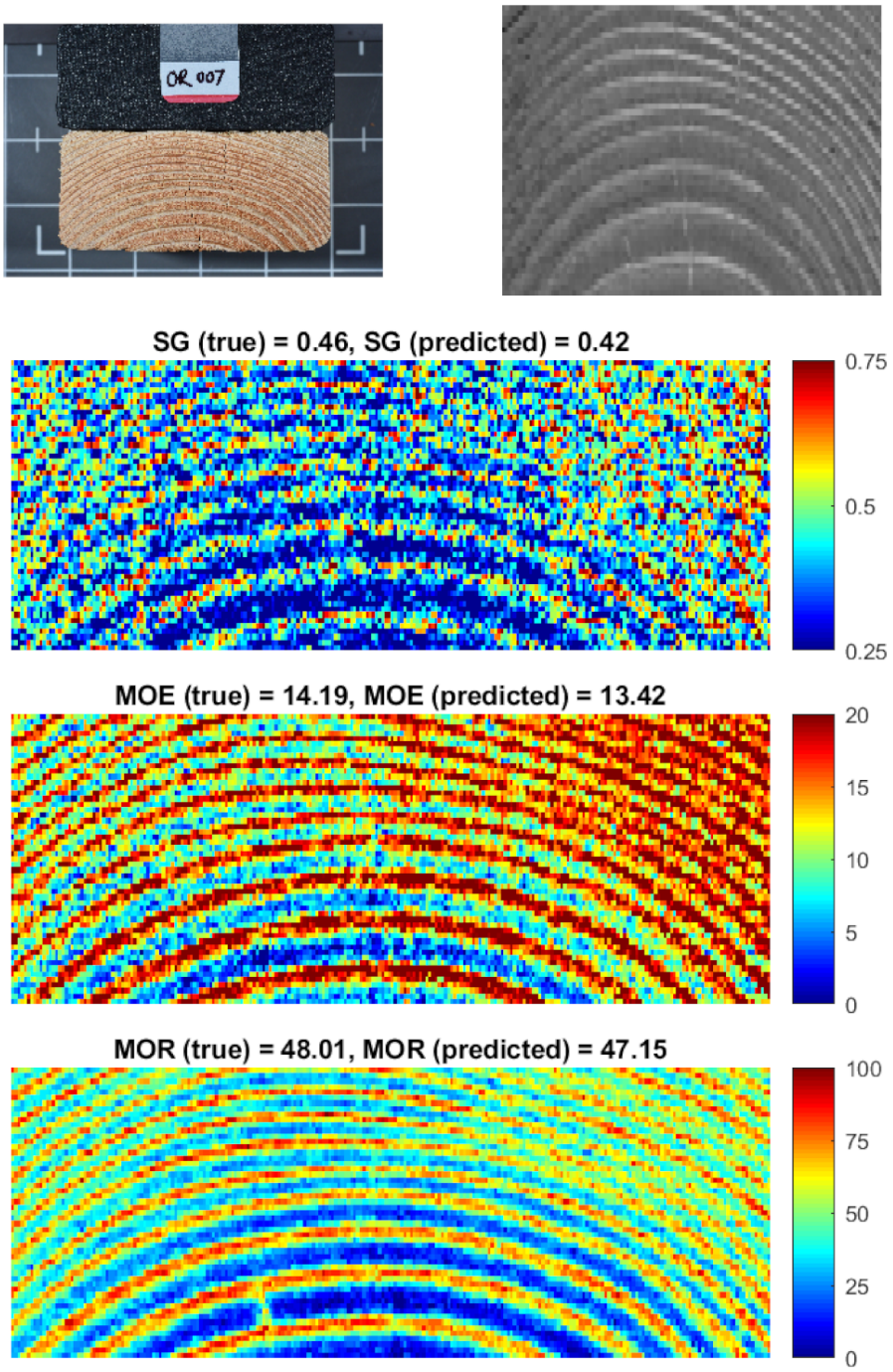

Figure 9. Top left: RGB image, **Top Right**: single hyperspectral channel image, **Bottom**: prediction of specific gravity (SG), modulus of elasticity (MOE) (GPa), and modulus of rupture (MOR) (MPa) using the PLS models and applied to one sample in the study with narrow growth rings.

4. Discussion

In efforts to utilize NIR spectroscopy to estimate lumber properties, various approaches have been employed, with the majority of studies collecting spectra along the length of the sample from either the radial face, tangential face, or somewhere between the two where neither a perfect radial or tangential face is available for examination, as is common in flatsawn lumber. The quality of information collected with reference to its suitability for estimation of whole lumber quality will vary between the two (radial vs tangential) extremes, with the radial face providing the most representative spectra and the tangential face the least [69]. In sawmill lumber with a very wide variety of orientations, ranging from

quartersawn to flatsawn and everything in between can be expected. Hence, scanning along the length of a board can provide spectra that potentially represent the properties of a board very well (when the radial face is scanned) to one that does not (when the tangential face is scanned), or does only partially (somewhere between radial and tangential), if scanning is done on only one face. Current automated grading systems employ cameras and sensors on all four faces, and given the cost of a hyperspectral camera, this type of setup is likely not feasible. For these reasons, we chose to scan the transverse face. The transverse face also demonstrates the variation in orientation described, but with this face, we can still accurately capture the variation in wood properties across rings; for example, the proportion of earlywood to latewood is visible on this face, which ultimately is an important factor in determining lumber properties such SG, MOE, and MOR.

To scan the transverse face, we utilized a FOSS benchtop NIR and NIR hyperspectral imaging (HSI) system. Scanning lumber on a benchtop NIR had been described previously [25], with promising results in that the NIR spectra was better correlated with wood stiffness than lumber SG. However, the use of the benchtop system presented problems because the authors calculated that the spectra collected represented less than 10% of the transverse area of the sample and thus failed to fully capture sample variability. Rather than collect more spectra per sample on the benchtop instrument in an attempt to better represent a board, a NIR-HSI system, which can quickly capture an image of the entire transverse surface, was explored. As each pixel has its own NIR spectrum, a representative whole-board spectrum can be obtained by averaging spectra across all pixels, which in principle should be more representative of the entire transverse surface. Despite improved representation of the surface, the two different approaches gave calibration/prediction results that were similar (Table 2), with FOSS NIR having slightly better calibration statistics, while predictions based on NIR-HSI data were marginally better, perhaps due to the greater area covered in the measurement. In a similar comparative study (FOSS XDS probe vs NIR-HSI) based on loblolly pine logs, similar results (SG and moisture content calibrations/predictions) for the two scanning options were also reported [48]. While we may have achieved greater coverage of the surface using NIR-HSI, we know the spectra are not of the same quality as a benchtop instrument, hence the lack of a substantial improvement in model performance.

We also explored the relationships between the SG, MOE, and modulus of rupture (MOR) and observed moderate results. For hard pines including southern pine (*Pinus* spp.), the relationship between SG and MOE, and to a lesser degree MOR, is known to be quite strong, particularly for short clear samples. In the southern pines, SG increases from pith to bark, while at the same time, microfibril angle decreases from pith to bark [70,71]. For Douglas-fir, the microfibril angle trend is the same as the southern pines, but SG decreases from pith to bark for approximately 10 years, then it gradually increases [67]. Thus, the relationships between SG and MOE and MOR is not as strong as what was reported previously for southern pine, and they mirror results others have found for Douglas-fir [72]. The presence of defects in lumber, particularly knots, will reduce the prediction accuracy of models in which defect information is not accounted for [73,74]. Here, we have no information on the defects within the lumber, and thus our models depend on the relative contributions of earlywood and latewood to estimate whole-board properties. Given the lack of information on knots in this study, the relationships reported here for the NIR benchtop and NIR-HSI calibrations may be approaching what can reasonably be expected for the NIR prediction of MOE or MOR. If the wood is very high quality (few knots, straight grain), then the calibration/prediction statistics may improve (e.g., Kobori et al. [30]); however, if the wood has numerous, large knots that detract greatly from the measured MOE and MOR, calibrations will suffer. Here, we used No. 2 grade lumber; if we had collected select structural lumber, we would likely have obtained better prediction statistics. Incorporation of defect information and the negative impact it has on wood properties could improve our prediction accuracy. Dahlen et al. [25] created a matrix which combined measured SG values with NIR data and created models using both measurements, which resulted in the improved accuracy of predictions of MOE (R_p^2 = 0.70) and MOR (R_p^2 = 0.52) compared to the NIR measurement alone for

MOE (R_p^2 = 0.58) and MOR (R_p^2 = 0.4) for southern pine. A similar idea could be explored with knot data, and it is likely that without it, NIR spectra (regardless of the face scanned) will fail to provide statistics that are much stronger than those reported here.

A strength of the NIR-HSI approach is that it allows the prediction of properties across the scanned surface, assuming an appropriate model exists. Here, we used our average spectra for whole-lumber PLS models for SG, MOE, and MOR to predict these properties of each pixel across the transverse surface of the scanned samples. This approach allowed us to visualize the variation in these properties within and among rings to be observed, particularly for samples with relatively wide rings, and we also observed the area at the pith as being of very low stiffness (Figure 8). For samples with narrow rings (Figure 9), it was more difficult to observe ring features owing to the similarity between ring and pixel size or the rings being smaller than the pixels. While this may be a concern for slowly grown conifers sourced from natural forests, it is not an issue for plantation-sourced trees that demonstrate much faster growth rates. The latter material is also where segregation becomes much more critical, because lumber pieces can consist entirely of corewood. We expect to see increasing mechanical properties from pith to bark, and the prediction variation we expect, as observed in Figures 8 and 9, i.e., very low MOE earlywood and very high MOE latewood, would be difficult to validate. Different approaches could be explored to help validate the data, for example measuring very small samples that contained only earlywood or latewood would help validate the general ranges predicted here; however, the approach would be extremely time-consuming and costly. Assuming we had the appropriate wood property data, a wide range of additional properties, such as wood chemistry information, as demonstrated by Thumm et al. [44,45], could have been generated.

How well our predictions of properties across the surface of a sample match actual measurements was not explored. In terms of within-ring and pith-to-bark variation, the predictions were consistent with our knowledge of SG, MOE, and MOR variation in conifers; however, further study is required to explore the accuracy of predictions. An instrument such as SilviScan [75] could be used to scan radial strips at a resolution equivalent to or greater than the pixel size for the NIR-HSI utilized in our study. While the approach we used to develop our calibrations (average the spectra and calibrate against a property measured on whole-piece basis, and then use the model to predict at high spatial resolution) has been utilized in other NIR-HSI studies, it is unknown what impact this approach has on the quality of predictions. As the calibration is based on data (lumber SG, MOE, and MOR) that has a range that is narrower than what it was used to predict (SG, MOE, and MOR variation within rings), then we expect that the model would both overestimate and underestimate the extremes.

We made no effort to improve the quality of the transverse surface of the samples prior to scanning, and the success of our models based on a reasonably rough surface indicates that the prediction of stiffness variation over the transverse surface of a log is feasible. Thumm et al. [44,45] have demonstrated the prediction of wood properties over a transverse surface (discs); however, they examined dry disks with surfaces that had been carefully prepared prior to scanning. Mora et al. [48] utilized green logs, and while they did not explore spatial variation (it was not an objective of their study), they had the required data. Potentially, spatial wood property data could be utilized in a mill to give an optimal sawing decision for a log aiming to maximize grade recovery, not just volume recovery. If implemented correctly, the value of such an approach could be considerable.

Exploration of options for manipulating information provided by NIR-HSI may also improve our ability to estimate lumber properties. For example, latewood and its proportion is an important determinate of SG, MOE, and MOR. If spectra from latewood regions of rings were weighted greater than earlywood when determining average spectra, it may improve our calibrations. Analysis of ring curvature could yield predictions of the location of the pith, which could allow for the estimation of the age of the material, which in turn would be insightful given the increasing trend of mechanical properties with cambial age. Further improvement in predictions could also be obtained by combining measurements; for example, the HSI information could be combined with the acoustic velocity of the log to refine predictions.

5. Conclusions

A NIR-HSI system and NIR benchtop instrument provided similar calibration and prediction statistics when used to rapidly estimate physical and mechanical properties of No. 2 2×4 Douglas-fir lumber. NIR-HSI data was used to examine SG, MOE, and MOR variation within and among rings. While the results are similar between the two systems, the use of a NIR-HSI system has several significant advantages over a typical NIR benchtop instrument, because of the greater versatility of the instrument and the ability to predict the spatial properties of a sample. In time, NIR-HSI may provide lumber mills with a cost-effective method to efficiently identify areas of high and low stiffness within logs prior to sawing, and thus would allow mills to make more informed decisions on a log-by-log basis for sawing solutions.

Supplementary Materials: The following are available online at http://www.mdpi.com/2076-3417/8/12/2602/s1.

Author Contributions: All authors designed the experiment. L.S. and J.D. wrote the original draft of the paper, with each of the coauthors contributing to subsequent versions. J.D. and S.-C.Y. analyzed the data.

Acknowledgments: This research was possible through support from NIFA McIntire-Stennis project 1006098. We would like to thank the reviewers and the handling editor, Byoung-Kwan Cho, for their helpful comments and suggestions in improving the manuscript.

Conflicts of Interest: The authors declare no conflict of interest.

References

1. Howard, J. *US Timber Production, Trade, Consumption, and Price Statistics 1965 to 2005*; Research Paper FPL-RP-637; U.S. Department of Agriculture, Forest Service, Forest Products Laboratory: Madison, WI, USA, 2007; p. 91.
2. Huang, C.L.; Briggs, D.G.; Lowell, E. Log lumber value of type II thinned Douglas-fir installations. In *Stand Management Cooperative quarterly news, 3rd Quarter*; School of Forest Resources, University of Washington: Seattle, WA, USA, 2011.
3. Azuma, D.L.; Bednar, L.F.; Heserote, B.A.; Veneklase, C.F. *Timber Resource Statistics for Western Oregon, 1997*; Resource Bulletin PNW-RB-237; U.S. Department of Agriculture, Forest Service, Pacific Northwest Research Station: Portland, OR, USA, 2004; p. 120.
4. Adams, W.T.; Hobbs, S.; Johnson, N. Intensively managed forest plantations in the Pacific Northwest, Conclusions. *J. For.* **2005**, *103*, 99–100.
5. Gray, A.N.; Veneklase, C.F.; Rhoads, R.D. *Timber Resource Statistics for Nonnational Forest Land in Western Washington, 2001*; Resource Bulletin PNW-RB-246; U.S. Department of Agriculture, Forest Service, Pacific Northwest Research Station: Portland, OR, USA, 2005; p. 117.
6. Talbert, C.; Marshall, D. Plantation productivity in the Douglas-fir region under intensive silvicultural practices: Results from research and operations. *J. For.* **2005**, *103*, 65–70.
7. Gartner, B.L. Assessing wood characteristics and wood quality in intensively managed plantations. *J. For.* **2005**, *103*, 75.
8. Vikram, V.; Cherry, M.L.; Briggs, D.; Cress, D.W.; Evans, R.; Howe, G.T. Stiffness of Douglas-fir lumber: Effects of wood properties and genetics. *Can. J. For. Res.* **2011**, *41*, 1160–1173. [CrossRef]
9. Moore, J.R.; Cown, D.J. Corewood (juvenile wood) and its impact on wood utilisation. *Curr. For. Rep.* **2017**, *3*, 107–118. [CrossRef]
10. Ross, R.J.; McDonald, K.A.; Green, D.W.; Schad, K.C. Relationship between log and lumber modulus of elasticity. *For. Prod. J.* **1997**, *47*, 89–92.
11. Wang, X.; Ross, R.J.; Mattson, J.A.; Erickson, J.R.; Forsman, J.W.; Geske, E.A.; Wehr, M.A. Nondestructive evaluation techniques for assessing modulus of elasticity and stiffness of small-diameter logs. *For. Prod. J.* **2002**, *52*, 79–86.
12. Carter, P.; Chauhan, S.; Walker, J. Sorting logs and lumber for stiffness using Director HM200. *Wood Fiber Sci.* **2006**, *38*, 49–54.
13. Wang, X. Acoustic measurements on trees and logs: A review and analysis. *Wood Sci. Technol.* **2013**, *47*, 965–975. [CrossRef]

14. Wang, X.; Verrill, S.; Lowell, E.; Ross, R.J.; Herian, V.L. Acoustic sorting models for improved log segregation. *Wood Fiber Sci.* **2013**, *45*, 343–352.
15. Moore, J.R.; Lyon, A.J.; Searles, G.J.; Lehneke, S.A.; Ridley-Ellis, D.J. Within- and between-stand variation in selected properties of Sitka spruce sawn timber in the UK: Implications for segregation and grade recovery. *Ann. For. Sci.* **2003**, *70*, 403–415. [CrossRef]
16. Butler, A.; Dahlen, J.; Eberhardt, T.L.; Montes, C.; Antony, F.; Daniels, R.F. Acoustic evaluation of loblolly pine tree- and lumber-length logs allows for segregation of lumber modulus of elasticity, not for modulus of rupture. *Ann. For. Sci.* **2017**, *74*, 20. [CrossRef]
17. Dahlen, J.; Montes, C.; Eberhardt, T.L.; Auty, D. Probability models that relate nondestructive test methods to lumber design values of plantation loblolly pine. *Forestry* **2018**, *91*, 295–306. [CrossRef]
18. Zhou, Z.-R.; Zhao, M.-C.; Wang, Z.; Wang, B.J.; Guan, X. Acoustic testing and sorting of Chinese poplar logs for structural LVL products. *BioResources* **2013**, *8*, 4101–4116. [CrossRef]
19. Achim, A.; Paradis, N.; Carter, P.; Hernández, R.E. Using acoustic sensors to improve the efficiency of the forest value chain in Canada: A case study with laminated veneer lumber. *Sensors* **2011**, *11*, 5716–5728. [CrossRef] [PubMed]
20. Gindl, W.; Teischinger, A.; Schwanninger, M.; Hinterstoisser, B. The relationship between near infrared spectra of radial wood surfaces and wood mechanical properties. *J. Near Infrared Spectrosc.* **2001**, *9*, 255–261. [CrossRef]
21. Kelley, S.S.; Rials, T.G.; Groom, L.H.; So, C.L. Use of infrared spectroscopy to predict the mechanical properties of six softwoods. *Holzforschung* **2004**, *58*, 252–260. [CrossRef]
22. Schimleck, L.R.; Jones, P.D.; Clark, A.; Daniels, R.F.; Peter, G.F. Near infrared spectroscopy for the nondestructive estimation of clear wood properties of *Pinus taeda* L. from the southern United States. *For. Prod. J.* **2005**, *55*, 21–28.
23. Haartveit, E.Y.; Flæte, P.O. Rapid prediction of basic wood properties by near infrared spectroscopy. *N. Z. J. For. Sci.* **2006**, *36*, 393.
24. Hein, P.R.G.; Brancheriau, L.; Trugilho, P.F.; Lima, J.T.; Chaix, G. Resonance and near infrared spectroscopy for evaluating dynamic wood properties. *J. Near Infrared Spectrosc.* **2010**, *18*, 443–454. [CrossRef]
25. Dahlen, J.; Diaz, I.; Schimleck, L.R.; Jones, P.D. Near-infrared spectroscopy prediction of southern pine No. 2 lumber physical and mechanical properties. *Wood Sci. Technol.* **2017**, *51*, 309–322. [CrossRef]
26. Hoffmeyer, P.; Pedersen, J.G. Evaluation of density and strength of Norway spruce by near infrared reflectance spectroscopy. *Holz Roh Werkst.* **1995**, *53*, 165–170. [CrossRef]
27. Meder, R.; Thumm, A.; Marston, D. Sawmill trial of at-line prediction of recovered lumber stiffness by NIR spectroscopy of *Pinus radiata* cants. *J. Near Infrared Spectrosc.* **2003**, *11*, 137–143. [CrossRef]
28. Fujimoto, T.; Kurata, Y.; Matsumoto, K.; Tsuchikawa, S. Application of near infrared spectroscopy for estimating wood mechanical properties of small clear and full length lumber specimens. *J. Near Infrared Spectrosc.* **2008**, *16*, 529–537. [CrossRef]
29. Fujimoto, T.; Kurata, Y.; Matsumoto, K.; Tsuchikawa, S. Feasibility of near-infrared spectroscopy for on-line grading of sawn lumber. *Appl. Spectrosc.* **2010**, *64*, 92–99. [CrossRef] [PubMed]
30. Kobori, H.; Inagaki, T.; Fujimoto, T.; Okura, T.; Tsuchikawa, S. Fast online NIR technique to predict MOE and moisture content of sawn lumber. *Holzforschung* **2015**, *69*, 329–335. [CrossRef]
31. Lu, G.; Fei, B. Medical hyperspectral imaging: A review. *J. Biomed. Opt.* **2014**, *19*, 010901. [CrossRef] [PubMed]
32. Elmasry, G.; Kamruzzaman, M.; Sun, D.W.; Allen, P. Principles and applications of hyperspectral imaging in quality evaluation of agro-food products: A review. *Crit. Rev. Food Sci. Nutr.* **2012**, *52*, 999–1023. [CrossRef]
33. Liu, Y.W.; Pu, H.B.; Sun, D.W. Hyperspectral imaging technique for evaluating food quality and safety during various processes: A review of recent applications. *Trends Food Sci. Technol.* **2017**, *69*, 25–35. [CrossRef]
34. Manley, M. Near-infrared spectroscopy and hyperspectral imaging: Non-destructive analysis of biological materials. *Chem. Soc. Rev.* **2014**, *43*, 8200–8214. [CrossRef]
35. Mishra, P.; Asaari, M.S.M.; Herrero-Langreo, A.; Lohumi, S.; Diezma, B.; Scheunders, P. Close range hyperspectral imaging of plants: A review. *Biosyst. Eng.* **2017**, *164*, 49–67. [CrossRef]
36. Burger, J.; Gowen, A. Data handling in hyperspectral image analysis. *Chemom. Intell. Lab. Syst.* **2011**, *108*, 13–22. [CrossRef]

37. Hagman, O. Multivariate prediction of wood surface features using an imaging spectrograph. *Holz Roh Werkst.* **1997**, *55*, 377–382. [CrossRef]
38. Nystrom, J.; Hagman, O. Real-time spectral classification of compression wood in *Picea abies*. *J. Wood Sci.* **1999**, *45*, 30–37. [CrossRef]
39. Duncker, P.; Spiecker, H. Detection and classification of Norway spruce compression wood in reflected light by means of hyperspectral image analysis. *IAWA J.* **2009**, *30*, 59–70. [CrossRef]
40. Jones, P.D.; Schimleck, L.R.; So, C.L.; Clark, A.; Daniels, R.F. High resolution scanning of radial strips cut from increment cores by near infrared spectroscopy. *IAWA J.* **2007**, *28*, 473–484. [CrossRef]
41. Fernandes, A.; Lousada, J.; Morais, J.; Xavier, J.; Pereira, J.; Melo-Pinto, P. Comparison between neural networks and partial least squares for intra-growth ring wood density measurement with hyperspectral imaging. *Comput. Electron. Agric.* **2013**, *94*, 71–81. [CrossRef]
42. Fernandes, A.; Lousada, J.; Morais, J.; Xavier, J.; Pereira, J.; Melo-Pinto, P. Measurement of intra-ring wood density by means of imaging VIS/NIR spectroscopy (hyperspectral imaging). *Holzforschung* **2013**, *67*, 59–65. [CrossRef]
43. Ma, T.; Inagaki, T.; Tsuchikawa, S. Calibration of SilviScan data of *Cryptomeria japonica* wood concerning density and microfibril angles with NIR hyperspectral imaging with high spatial resolution. *Holzforschung* **2017**, *71*, 341–347. [CrossRef]
44. Thumm, A.; Riddell, M.; Nanayakkara, B.; Harrington, J.; Meder, R. Near infrared hyperspectral imaging applied to mapping chemical composition in wood samples. *J. Near Infrared Spectrosc.* **2010**, *18*, 507–515. [CrossRef]
45. Thumm, A.; Riddell, M.; Nanayakkara, B.; Harrington, J.; Meder, R. Mapping within-stem variation of chemical composition by near infrared hyperspectral imaging. *J. Near Infrared Spectrosc.* **2016**, *24*, 605–616. [CrossRef]
46. Meder, R.; Meglen, R.R. Near infrared spectroscopic and hyperspectral imaging of compression wood in *Pinus radiata* D. Don. *J. Near Infrared Spectrosc.* **2012**, *20*, 583–589. [CrossRef]
47. Thumm, A.; Riddell, M. Resin defect detection in appearance lumber using 2D NIR spectroscopy. *Eur. J. Wood Wood Prod.* **2017**, *75*, 995–1002. [CrossRef]
48. Mora, C.; Schimleck, L.R.; Yoon, S.C.; Thai, C.N. Determination of basic density and moisture content of loblolly pine wood disks using a near-infrared hyperspectral imaging system. *J. Near Infrared Spectrosc.* **2011**, *19*, 401–409. [CrossRef]
49. Haddadi, A.; Burger, J.; Leblon, B.; Pirouz, Z.; Groves, K.; Nader, J. Using near-infrared hyperspectral images on subalpine fire board. Part 1: Moisture content estimation. *Wood Mater. Sci. Eng.* **2015**, *10*, 27–40. [CrossRef]
50. Haddadi, A.; Burger, J.; Leblon, B.; Pirouz, Z.; Groves, K.; Nader, J. Using near-infrared hyperspectral images on subalpine fire board. Part 2: Density and basic specific gravity estimation. *Wood Mater. Sci. Eng.* **2015**, *10*, 41–56. [CrossRef]
51. Lestander, T.A.; Geladi, P.; Larsson, S.H.; Thyrel, M. Near infrared image analysis for online identification and separation of wood chips with elevated levels of extractives. *J. Near Infrared Spectrosc.* **2012**, *20*, 591–599. [CrossRef]
52. Dahlen, J.; Jones, P.D.; Seale, R.D.; Shmulsky, R. Mill variation in bending strength and stiffness of in-grade Douglas-fir No. 2 2 × 4 lumber. *Wood Sci. Technol.* **2013**, *47*, 1167–1176. [CrossRef]
53. ASTM International. *ASTM D4761-13: Standard Test Methods for Mechanical Properties of Lumber and Wood-Base Structural Material*; ASTM International: West Conshohocken, PA, USA, 2013.
54. ASTM International. *ASTM D198-15: Standard Test Methods of Static Tests of Lumber in Structural Sizes*; ASTM International: West Conshohocken, PA, USA, 2015.
55. ASTM International. *ASTM D1990-16: Standard Practice for Establishing Allowable Properties for Visually-Graded Dimension Lumber from in-Grade Tests of Full-Size Specimens*; ASTM International: West Conshohocken, PA, USA, 2016.
56. R Core Team. *R: A Language and Environment for Statistical Computing*; R Foundation for Statistical Computing: Vienna, Austria, 2018; Available online: http://www.R-project.org/ (accessed on 18 April 2018).
57. RStudio. *RStudio: Integrated Development Environment for R*; RStudio: Boston, MA, USA, 2018; Available online: https://www.rstudio.com/ (accessed on 18 April 2018).

58. Auguie, B. gridExtra: Miscellaneous Functions for "grid" Graphics. R Package Version 2.2.1. 2016. Available online: https://CRAN.R-project.org/package=gridExtra (accessed on 18 April 2018).
59. Mevik, B.-H.; Wehrens, R.; Liland, K.H. pls: Partial Least Squares and Principal Component Regression. R Package Version 2.4-3. 2013. Available online: http://CRAN.R-project.org/package=pls (accessed on 18 April 2018).
60. Stevens, A.; Ramirez-Lopez, L. An Introduction to the Prospectr Package. R Package Vignette R Package Version 0.1.3. 2013. Available online: https://cran.r-project.org/web/packages/prospectr/vignettes/prospectr-intro.pdf (accessed on 18 April 2018).
61. Signal Developers Signal: Signal Processing. 2013. Available online: http://r-forge.r-project.org/projects/signal/ (accessed on 18 April 2018).
62. Wickham and Rstudio Tidyverse: Easily Install and Load the 'Tidyverse' R Package Version 1.2.1. 2017. Available online: https://cran.r-project.org/web/packages/tidyverse/index.html (accessed on 18 April 2018).
63. Savitzky, A.; Golay, M.J.E. Smoothing and differentiation of data by simplified least squares procedures. *Anal. Chem.* **1964**, *36*, 1627–1639. [CrossRef]
64. Snee, R.D. Validation of regression models: Methods and examples. *Technometrics* **1977**, *19*, 415–428. [CrossRef]
65. Mora, C.; Schimleck, L.R. On the selection of samples for multivariate regression analysis: Application to near infrared (NIR) calibration models. *Can. J. For. Res.* **2008**, *38*, 2626–2634. [CrossRef]
66. Williams, P.C.; Sobering, D.C. Comparison of commercial near infrared transmittance and reflectance instruments for the analysis of whole grains and seeds. *J. Near Infrared Spectrosc.* **1993**, *1*, 25–32. [CrossRef]
67. Kimberley, M.O.; McKinley, R.B.; Cown, D.J.; Moore, J.R. Modelling the variation in wood density of New Zealand-grown Douglas-fir. *N. Z. J. For. Sci.* **2017**, *47*, 15. [CrossRef]
68. *AACC 39-00.01, Near-Infrared Methods—Guidelines for Model Development and Maintenance*; AAAC International: St. Paul, MN, USA, 1999.
69. Schimleck, L.R.; Matos, J.L.M.; Trianoski, R.; Prata, J.G. Comparison of methods for estimating mechanical properties of wood by NIR spectroscopy. *J. Spectrosc.* **2018**, 4823285. [CrossRef]
70. Jordan, L.; He, R.; Hall, D.B.; Clark, A.; Daniels, R.F. Variation in loblolly pine ring microfibril angle in the Southeastern United States. *Wood Fiber Sci.* **2007**, *39*, 352–363.
71. Jordan, L.; Clark, A.; Schimleck, L.R.; Hall, D.; Daniels, R.F. Regional variation in wood specific gravity of planted loblolly pine in the United States. *Can. J. For. Res.* **2008**, *38*, 698–710. [CrossRef]
72. Filipescu, C.N.; Stoehr, M.U.; Pigott, D.R. Variation of lumber properties in genetically improved full-sib families of Douglas-fir in British Columbia, Canada. *Forestry* **2018**, *3*, 320–326. [CrossRef]
73. Roblot, G.; Bléron, L.; Mériaudeau, F.; Marchal, R. Automatic computation of the knot area ratio for machine strength grading of Douglas-fir and Spruce timber. *Eur. J. Environ. Civ. Eng.* **2010**, *14*, 1317–1332. [CrossRef]
74. Butler, M.A.; Dahlen, J.; Antony, F.; Kane, M.; Eberhardt, T.L.; Jin, H.; Love-Myers, K.; McTague, J.P. Relationships between loblolly pine small clear specimens and dimension lumber tested in static bending. *Wood Fiber Sci.* **2016**, *48*, 81–95.
75. Evans, R. Wood stiffness by x-ray diffractometry. In *Characterization of the Cellulosic Cell Wall*; Stokke, D.G., Groom, L., Eds.; Blackwell Publishing: Ames, IA, USA, 2006; pp. 138–146.